

Easily Coupled Whispering Gallery Plasmons in Dielectric Nanospheres Embedded in Gold Films

R. M. Cole, Y. Sugawara, and J. J. Baumberg

School of Physics and Astronomy, University of Southampton, Highfield, Southampton, SO17 1BJ, United Kingdom

S. Mahajan, M. Abdelsalam, and P. N. Bartlett

School of Chemistry, University of Southampton, Highfield, Southampton, SO17 1BJ, United Kingdom

(Received 24 July 2006; published 25 September 2006)

A new self-aligned robust method for coupling to whispering gallery modes (WGMs) of submicron microspheres utilizes their periodic arrangement without relying on nanopositioned external coupling devices. The microspheres are embedded in a nanostructured gold surface supporting delocalized plasmonic crystal modes that mediate the coupling, and can be tuned by the geometry. Detailed measurements of the angle- and orientation-dependent reflectivity reveal localized plasmonic WGMs whose energies scale with sphere diameter and agree closely with Mie calculations. Coupling between these plasmonic WGMs leads to mode splitting and the formation of plasmonic minibands of a controllable bandwidth.

DOI: [10.1103/PhysRevLett.97.137401](https://doi.org/10.1103/PhysRevLett.97.137401)

PACS numbers: 78.67.Bf, 42.70.Qs, 73.20.Mf, 81.07.-b

Microspheres form one of the key elements in nanophotonic devices due to the tight confinement and strong enhancement of the optical field. However, coupling into microspheres is difficult due to the weak exponentially decaying evanescent external field, and has been demonstrated only with nanopositioned elements such as prisms [1,2], modified optical fiber probes (using tapers [3], etched-eroded [4] or angle-polished [5] fiber tips, half-block fiber couplers), or planar waveguides [6]. These methods require precise nanometer control in the optical near field, placing tight tolerance on alignment and fabrication. Current whispering gallery mode (WGM) research has tended to focus on large dielectric microspheres (from several to hundreds of microns) with high Q factors and which support many closely spaced modes of very narrow linewidth. This mode quasidegeneracy and the large size restricts applications, for instance, in coupling to small numbers of nanoemitters. Additionally, microspheres are frequently supported on flat or grooved substrates, with the outer surface in air or liquid, providing limited scope for control of interactions. Because of the difficulty of matched coupling, most studies collect photoluminescence (PL) from dye-doped spheres in which small numbers of spheres can be resolved although the excitation conditions are not well controlled [7–9].

Here we demonstrate for the first time strong WGM resonances in embedded spheres with submicron diameters. Since the sphere dimensions (diameters $d = 0.4$ to $1 \mu\text{m}$) are comparable to the wavelength of illuminating light we observe the lowest order WGM modes directly. These modes can be observed in reflectivity through the entire visible and IR spectral ranges and are conveniently widely spaced energetically. By using a far-field resonant coupling method only possible for such embedded microspheres in a metal film, we can study the full angular dependence of these modes and observe the mode linewidths and absorption depths directly as the film thickness

is varied. The observed localized modes combine aspects of both WGMs and void plasmons [10,11] as their angular mode index, l , changes and hence are termed *plasmonic* WGMs below. We clearly resolve the evolution from delocalized surface plasmons (with bands), to individual plasmonic WGM modes (localized), to local plasmon hopping between neighboring microspheres (giving minibands).

The embedded sphere samples are produced via a template self-assembly and electrochemical deposition technique that allows a number of metals (here gold) to be grown conformally around an array of latex spheres (diameter d) [12,13]. Grading the thickness, t , of encapsulating gold along the cm-scale length of each sample, allows investigation of normalized thicknesses $\bar{t} = t/d$ from flat gold $\bar{t} = 0$ to complete encapsulation at $\bar{t} = 1$ by scanning the illuminated spot (Fig. 1). A supercontinuum white-light laser provides spectral illumination from 480 nm to $2 \mu\text{m}$ and allows high angular resolution from small sample regions. An automated goniometer controls the sample orientation and measures the reflectivity spectrum for incident angles, θ , from normal incidence 0° to 80° , sample azimuthal orientations, $\phi = 0^\circ$ to 360° , and varying thickness \bar{t} . Spectra are recorded using visible and infrared spectrometers, while polarizing optics are employed to distinguish s - and p -polarized reflected light. Reconstruction of these full experimental dispersion relations is crucial to characterize and identify the modes in such nanostructured films.

Our samples support a rich variety of both localized plasmonic WGM modes and delocalized surface modes, evident in the typical experimental dispersions for spheres of diameter $d = 600$ and 900 nm (Fig. 2). Thin samples $\bar{t} \sim 0$ [Figs. 2(b) and 2(f)] produce mode energies strongly dependent on their in-plane wave vector, characteristic of delocalized propagation. Good agreement is found be-

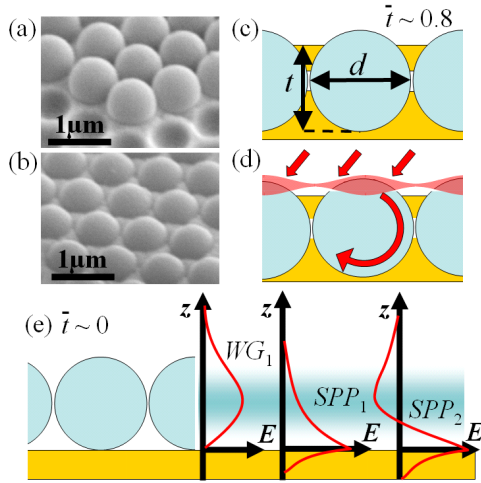


FIG. 1 (color online). (a), (b) Angled electron micrographs of $d = 700$ nm spheres at (a) $\bar{t} = 0.15$, (b) $\bar{t} = 0.55$. (c) Schematic film cross-section for normalized thickness $\bar{t} = t/d$ for thickness, t , and diameter, d of $\bar{t} = 0.8$. (d) Schematic SPP coupling to WGM. (e) Schematic field profiles for first waveguide mode, WG_1 , first surface plasmon mode, SPP_1 , and second surface plasmon mode, SPP_2 .

tween the observations and a simple theory based on an empty-lattice approximation which zone folds the band structure [Figs. 2(a) and 2(e)]. Three principal modes are seen with effective refractive indices \bar{n} corresponding to the waveguide mode WG_1 (black lines, $\bar{n} \sim 1.6$) formed by the touching spheres, the first order surface plasmon mode SPP_1 (blue dotted curves, $\bar{n} \sim 1.0$) tied to the metal surface, and the second-order surface plasmon mode SPP_2 [gray curves (red online), $\bar{n} \sim 1.4$] tied to the metal surface but extending further into the spheres [see $E(z)$, Fig. 1(e)]. These delocalized modes exhibit a clear sixfold symmetry in azimuthal measurements with ϕ (not shown) [11]. The WG_1 and SPP_2 modes have significant field strength within the periodic sphere layer, and hence are more efficiently diffractively coupled than the SPP_1 mode for thicknesses $\bar{t} < 0.5$. We note that the planar waveguide mode WG_1 formed by the chains of touching spheres has been previously termed a “nanojet” mode in 1D propagation [14].

As the thickness of gold is increased from $\bar{t} = 0$, the area of surface available to the SPP_1 mode is reduced and it temporarily disappears from the data around $\bar{t} = 0.5$, reappearing only around $\bar{t} \sim 1$. Similarly, the WG_1 mode becomes occluded when the gold reaches half the sphere height and is no longer directly coupled. In contrast, the second-order SPP_2 mode which originates at the gold surface breaks apart into discrete nondispersive modes by $\bar{t} = 0.5$, seen in both s and p polarizations [Figs. 2(c), 2(d), 2(g), and 2(h)]. The energies of these discrete modes which are independent of ϕ match well with calculations of the plasmonic WGMs inside microspheres of refractive index $n = 1.6$ embedded inside gold (also shown in Fig. 2). Together with the θ independence of the mode energy (clearest in s polarizations) seen for thicknesses

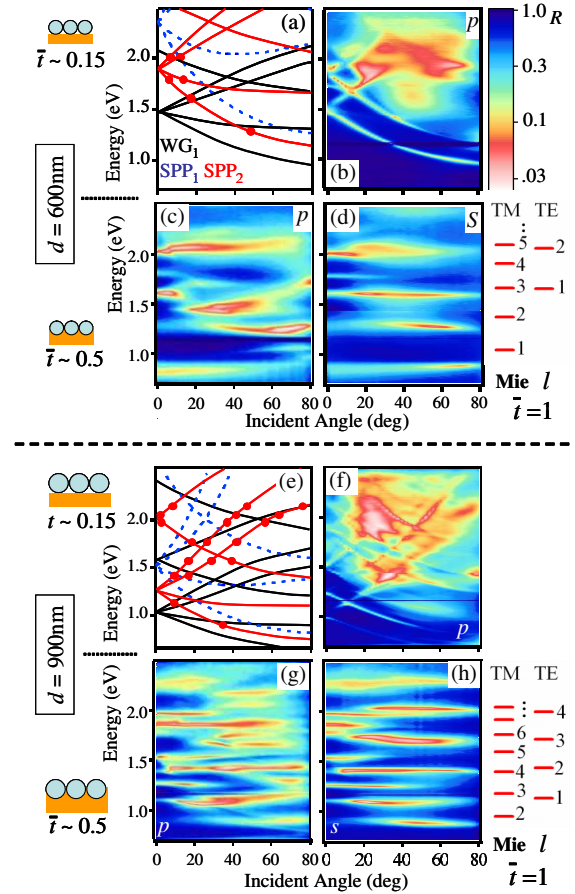


FIG. 2 (color online). Dispersion relations, $E(\theta)$, with $\phi = 0^\circ$ for sphere diameters $d = 600$ nm and 900 nm: (a), (e) band theory of WG_1 (black), SPP_1 (blue dashed) and SPP_2 [gray (red online)] modes on flat gold interface. Points show intersection of SPP_2 dispersion with localized Mie modes. Measured reflectivity dispersions (on log scale, normalized to flat Au) for (b), (f) p polarization at $\bar{t} = 0.15$, (c), (g) p polarization at $\bar{t} = 0.50$, (d), (h) s polarization at $\bar{t} = 0.50$. Plasmonic WGM energies calculated from Ref. [10].

$0.4 < \bar{t} < 1$, this behavior confirms the localized nature of these modes inside the spheres.

The mode assignment is further supported by extracting the dominant mode energies for a range of samples with nominal sphere diameters from $d = 0.6$ to $1 \mu\text{m}$ at $\bar{t} > 0.5$ which all show similar features (Fig. 3). As discussed below, modes absorb strongly at different angles, hence individual spectra show particular patterns of peaks [Fig. 3(a)] [15]. The extracted modes are compared to theoretical mode calculations, $E_l(d)$, in the perfect spherical void, calculated by matching boundary conditions at the void rim using the full frequency-dependent dielectric constant for gold [10]. Evidence is seen for mixing between near-degenerate TE and TM solutions, produced by the complex 3D hemispherical surface geometry. However, the simple theory reproduces well the observed trends and mode spacings with d and l .

These plasmonic WGMs bridge the space between traditional WGMs, Fabry-Perot modes, and localized void

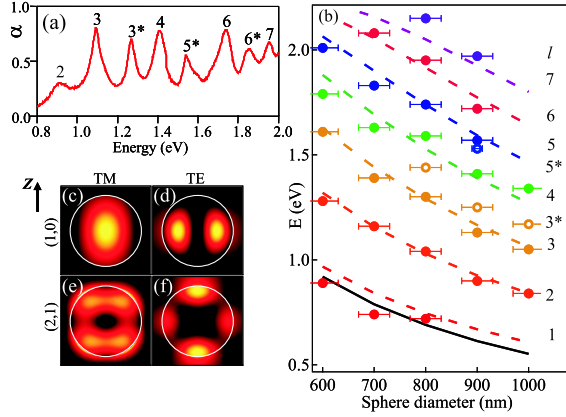


FIG. 3 (color online). (a) Absorption spectrum $\alpha = 1 - R$, of $d = 900$ nm sample at $\bar{t} = 0.6$, $\theta = 25^\circ$, $\phi = 0^\circ$, and s polarization. (b) Observed WGM energies vs sphere diameter, together with the calculated dependence of TM modes (dashed lines, labeled by radial mode number l). Theoretical limit of diffractive coupling (black line) also shown. (c), (d), (e), (f) Corresponding computed field profiles in xz plane (rotationally symmetric about the z axis) for $(l, m) = (1, 0)$ and TM , TE polarizations.

plasmons. Each mode is classified by integral indices n , l , m which are the radial, angular and azimuthal mode numbers, respectively. In the perfect spherical void the mode energy is independent of m , while the modes with $n > 1$ occur at high energy and do not clearly appear in the data. However, due to their different boundary conditions, the modes with TE and TM polarization have different energies. As $d \rightarrow \infty$, the TM large- l solutions tend to the conventional SPPs on flat gold, while the TE modes resemble the Fabry-Perot modes of spherical microcavities with field nodes at the metal surfaces (and thus they disappear on the flat surface). The TM mode intensity distributions [Figs. 3(c) and 3(e)] resemble those of the spherical angular harmonics, $Y_{l-1,m}(\theta, \phi)$, increasingly bound closer to the metal walls at higher l [16]. While this simple treatment ignores the influence of the varying gold height encapsulation as well as the interaction with neighboring spheres, it provides the appropriate basis states to understand the system.

We now discuss the mechanism of efficient coupling between plane wave incident light and these plasmonic WGMs for $\bar{t} > 0.4$. We concentrate on s -polarized absorption on thick samples which highlights the uncoupled WGMs, since for p polarizations the neighboring WGMs can couple through the intervening metal surface which supports SPPs. Clues to the coupling mechanism are given by the angle dependence of the discrete WGMs [Figs. 2(d) and 2(h)] which shows that the optimal incident angle varies systematically depending on the mode energy. This provides strong evidence that coupling proceeds by diffractive coupling to the SPP_2 mode which is already localized inside the dielectric spheres and effectively mixed with the plasmonic WGM [Fig. 1(d)]. Essentially, the dispersion is a convolution of the discrete Mie energies

of Figs. 2(d) and 2(h), with the surface-mediating plasmons SPP_2 of Figs. 2(a) and 2(e), marked as the solid points. The limiting condition for diffractive coupling (at $\theta = 90^\circ$) is given by [Fig. 3(b), solid line]:

$$E_l(d) > \frac{4\pi\hbar c}{d\sqrt{3}(1+\bar{n})} \quad (1)$$

which is satisfied even for $l = 1$, for all sphere sizes. Such diffractive coupling to low-order WGMs only works because of the surrounding metal which provides the delocalized plasmon.

The energy, absorption depth, spectral and angular linewidths are extracted from the measured dispersions for each thickness and diameter, allowing a detailed characterization of the plasmonic WGMs. The broad angular widths ($\Delta\theta \sim 5\text{--}20^\circ$) observed imply that the delocalized SPPs travel only a few microns before their energy is transferred into the localized WGMs. The linewidth (and hence Q factor) as well as the absorption depth are seen to only weakly depend on the encapsulation \bar{t} of the spheres. Between $0.6 < \bar{t} < 0.8$ the plasmonic WGM modes are further broadened, which we believe may be associated with their mixing to the triangular metal islands in the interstices between the microspheres [11]. The mode Q factors reach a maximum of 30 for $\bar{t} \sim 0.95$ where radiative losses are suppressed by the small aperture. The WGMs attain maximum absorption strengths of up to 98%. While both linewidth and absorption strengths are not fully understood (since no theoretical model is yet capable of modelling such structures), we believe that the linewidths are currently limited by the 2% size inhomogeneity of the spheres, rather than radiative, absorptive, and coupling losses.

As well as observing delocalized plasmon modes (analogous to electronic nearly free electron bands), and localized plasmons (analogous to atomic orbitals), we identify nearest-neighbor coupling between plasmonic WGMs (analogous to tight-binding electronic bands). Coupling between spheres can occur either via the top metal surface or through small circular windows formed between the spheres (due to screening during electrodeposition within the microsphere geometry [16]). By uniformly coating the samples with an extra 6 nm of sputtered gold, we selectively modify this coupling. Hopping of localized plasmons between WGMs in neighboring spheres can be identified from the formation of minibands in the dispersion. Dielectric microsphere coupling has been identified recently in one dimension [7] from the PL emitted by larger $4 \mu\text{m}$ spheres stacked in a line. While such experiments allow only the discrete states to be observed as a function of the number of spheres in the chain, we are able here to fully map the dispersion using angle-dependent reflectivity, directly revealing the minibands.

Typical coupling data for the plasmon WGMs, shown for thicker films with $d = 900$ nm (Fig. 4), reveals the complex dispersion in the uncoated spheres resulting from the mixing of the $2(l+1)$ degenerate modes at

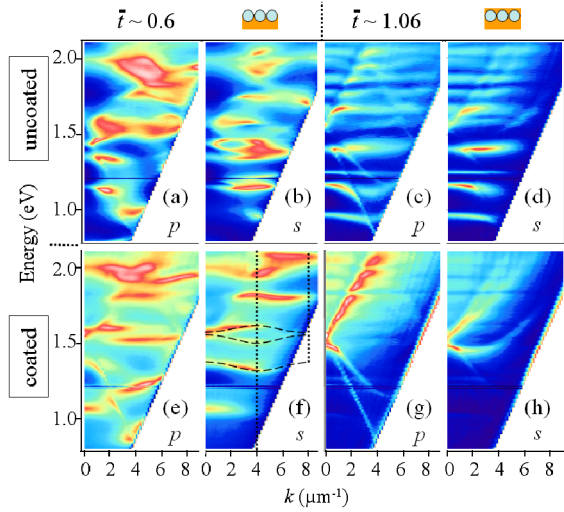


FIG. 4 (color online). Experimental s , p dispersions $E(k)$ for sphere diameter $d = 900$ nm at thicknesses $\bar{t} = 0.6$ and 1.06 using (a), (b), (c), (d) uncoated spheres and (e), (f), (g), (h) spheres overcoated with 6 nm of gold. Dashed lines in (f) show minibands.

each $E_l(d)$. For barely encapsulated spheres ($\bar{t} = 1.06$) coupling to the Mie modes is evident, together with SPP₁ modes on the top surface which are only strong when near-degenerate to these Mie modes [Figs. 4(c) and 4(d)]. For smaller thicknesses the modes split and mix in complex ways. However, in the coated sphere samples this coupling is clearly reduced: the extra electromagnetic barrier formed by the 6 nm coating suppresses mixing between low l modes whose fields do not penetrate and overlap with either top surface or neighboring spheres. Measurements at precisely the same points before and after coating show clearly this reduced coupling retaining only the SPP₁ mode for $\bar{t} = 1.06$ [Figs. 4(g) and 4(h)].

For thinner embedding layers [Figs. 4(e) and 4(f)] a number of new effects can be identified. The surface plasmons are once again visible in p polarization, presumably propagating *over* the hemispherical domes [Fig. 1(b)]. Minibands appear [Fig. 4(f)], with dispersions following a tight-binding model, $E_k = E_l' + 2g \cos(ka)$ with Brillouin zone boundary, $k_{BZ} = \pi/a = 4.0 \mu\text{m}^{-1}$ (dashed vertical line) and coupling strength, g , controlled by the mode overlap between spheres (which increases with l). Finally we observe mixing of Bragg modes and minibands in p polarization [Fig. 4(e)]. Although no theory currently exists for such tight-binding calculations in a 2D triangular lattice for confined vectorial fields with different l , the reasonable fit to a 1D linear model suggests that such a development is attainable. The full evolution of these plasmonic WGM modes as the thickness of both film and coating are systematically varied gives some insight into how the coupling proceeds: for $\bar{t} \sim 0.5$ or 1 , the WGM modes remain rather stable whereas for $\bar{t} \sim 0.75$ or 0.25 they display a great sensitivity to \bar{t} . This suggests that modes with field profiles which overlap with the upper

metal surface [e.g., Fig. 3(e)] are most involved in plasmonic hopping, and also that the metal surfaces are crucial in effecting this interaction. Such behavior shows that interactions between plasmon WGMs can be clearly controlled by the geometry of nanostructured sphere samples.

In summary, we demonstrate self-aligned robust coupling to plasmon whispering gallery modes in submicron spheres which utilizes their periodic arrangement and does not rely on nanopositioned external coupling devices. We map the full set of modes in such microspheres through their angular-dependent reflectivity and show that interaction between delocalized surface modes and localized WGM modes is crucial for efficient coupling. Control of the metal thickness in which the spheres are embedded allows the couplings to be tuned, as well as the properties of the plasmonic WGMs to be optimized. Plasmon hopping between neighboring spheres is also identified, forming minibands. Such localized plasmonic WGMs are useful in a range of applications such as sensors and microlasers, as well as novel matched emitters and absorbers.

We enthusiastically acknowledge discussions with Javier Garcia de Abajo. This work was supported by EPSRC Grant No. EP/C511786/1. Y. S. was supported by JSPS through Grant No. HEISEI 15.

-
- [1] A. Pipino, J. Hudgens, and R. Huie, *Rev. Sci. Instrum.* **68**, 2978 (1997).
 - [2] Y. Pan and R. K. Chang, *Appl. Phys. Lett.* **82**, 487 (2003).
 - [3] J. Laine, B. E. Little, and H. A. Haus, *IEEE Photonics Technol. Lett.* **11**, 1429 (1999).
 - [4] Y. P. Rakovich, J. F. Donegan, M. Gerlach, A. L. Bradley, T. M. Connolly, J. J. Boland, N. Gaponik, and A. Rogach, *Phys. Rev. A* **70**, 051801(R) (2004).
 - [5] V. S. Ilchenko, X. S. Yao, and L. Maleki, *Opt. Lett.* **24**, 723 (1999).
 - [6] M. Cai, O. Painter, and K. J. Vahala, *Phys. Rev. Lett.* **85**, 74 (2000).
 - [7] T. Mukaiyama, K. Takeda, H. Miyazaki, Y. Jimba, and M. Kuwata-Gonokami, *Phys. Rev. Lett.* **82**, 4623 (1999).
 - [8] R. Jia, D. Jiang, P. Tan, and B. Sun, *Appl. Phys. Lett.* **79**, 153 (2001).
 - [9] V. N. Astratov, J. P. Franchak, and S. P. Ahhili, *Appl. Phys. Lett.* **85**, 5508 (2004).
 - [10] S. Coyle *et al.*, *Phys. Rev. Lett.* **87**, 176801 (2001).
 - [11] T. A. Kelf, Y. Sugawara, J. J. Baumberg, M. Abdelsalam, and P. N. Bartlett, *Phys. Rev. Lett.* **95**, 116802 (2005).
 - [12] P. Bartlett, J. J. Baumberg, P. Birkin, M. Ghanem, and M. Netti, *Chem. Mater.* **14**, 2199 (2002).
 - [13] P. Bartlett, J. J. Baumberg, S. Coyle, and M. Abdelsalam, *Faraday Discuss.* **125**, 117 (2004).
 - [14] Z. Chen, A. Taflove, and V. Backman, *Opt. Lett.* **31**, 389 (2006).
 - [15] Note that the minima in reflectivity that we identify correspond to zeros, not poles, of the complex reflectivity; however, these are very close in energy.
 - [16] T. A. Kelf, Y. Sugawara, R. M. Cole, J. J. Baumberg, M. Abdelsalam, S. Cintra, S. Mahajan, A. E. Russell, and P. N. Bartlett, *Phys. Rev. B* (to be published).